



Heat and Mass Transfer Enhancement in Absorption of Vapor in Laminar Liquid Film by Adding Nano-Particles

S. Armou[†], R. Mir, Y. El Hammami, K. Zine-Dine and M. El Hattab

*Laboratory of Mechanics, Processes, Energy and Environment, National School of Applied Sciences
 ENSA, B.P 1136, Agadir, Morocco*

[†]Corresponding Author Email: sara.armou@gmail.com

(Received November 3, 2016; accepted June 13, 2017)

ABSTRACT

In this paper, a numerical study was performed. The effect of nanoparticles on the absorption of vapor into a liquid film of lithium bromide aqueous solution flowing down over a cooled vertical channel is examined. The present model uses the numerical finite volume method to solve the parabolic governing equations for two-dimensional and laminar flow. In this model, the cooling water flows countercurrent to a solution of concentrated lithium bromide mixed with the nanoparticles. The water vapor is then absorbed at the interface of the absorbent film and diffused into the binary nanofluid (water-LiBr+nanoparticles). The numerical results indicate that the mass and heat transfer in binary nanofluids are enhanced more than that in base fluid and the highest absorption mass flux is observed by adding argent (Ag) nanoparticles. The results of the effects of operating conditions show that the effectiveness of the nanofluid becomes higher than that with the base fluid when the Reynolds number and inlet concentration are lower and when the inlet temperature solution and inlet pressure are higher.

Keywords: Heat transfer; Mass transfer; Enhancement; Absorption process; Falling film; Water-Lithium bromide; Nanoparticles; Numerical simulation.

NOMENCLATURE

c_p	specific heat of solution	x	coordinate perpendicular to the flow
D	mass diffusivity coefficient	y	coordinate in direction flow
g	gravitational acceleration		
h_{abs}	heat of absorption	δ	film thickness
h	heat transfer coefficient	φ	solid volume fraction
h_m	mass transfer coefficient	ρ	density
H	absorber plate width	μ	dynamic viscosity
k	thermal conductivity	Γ	liquid film flow rate
L	length of absorber		
M	average mass flux		
\dot{m}	absorption mass flux	subscripts	
Nu	Nusselt number	<i>abs</i>	absorption
P	pressure	<i>bw</i>	bulk solution to wall plate
Q	average heat flux	<i>c</i>	cooling water
q	heat flux	<i>f</i>	fluid
Re	Reynolds number	<i>in</i>	inlet
Sh	Sherwood number	<i>ib</i>	interface to bulk solution
T	temperature	<i>nf</i>	nanofluid
u	velocity in x-direction of the liquid solution	<i>out</i>	outlet
v	velocity in y-direction of the liquid solution	<i>p</i>	particle
W	mass fraction LiBr in solution	<i>surf</i>	liquid-vapor interface
		<i>w</i>	wall

1. INTRODUCTION

The absorption refrigeration system has been broadly used in many applications as air conditioning, the absorber is the most critical component in the absorption machines by using LiBr-H₂O and NH₃-H₂O as refrigerant-absorbent mixtures where the refrigerant vapor is absorbed into the absorbent liquid in falling film. So to enhance the performance of the absorption system, it is recommended to examine the characteristics of heat and mass transfer in the absorber.

A nanofluid is defined as a dilute suspension of metallic and non-metallic nanoparticles with nanometric size below 100nm in a base fluid such as oil, water and ethylene glycol. Recently, nanofluids have been emerged extensively as a nano-technology to enhance the heat transfer rate. Many experimental researches have been published with regards to the effect of nanofluid on heat and mass transfer performance in the absorption system. Kim *et al.* (2006) examined experimentally the effect of nanoparticles on the bubble absorption performance of NH₃-H₂O system. The results showed that the addition of 0.10% of Cu nanoparticles and 18.7% of ammonia solution make the absorption ratio greater 3.21 times. Moreover, the effectiveness of the nanofluid increases with the increasing of the initial concentration of ammonia solution and as well as the addition of nanoparticles is more effective with a low absorption potential. The enhanced mass transfer during the ammonia-water bubble absorption is studied experimentally by Pang *et al.* (2012), Mono silver (Ag) nanoparticles were used to produce the binary nanofluids for application of NH₃-H₂O absorption in a bubble absorber. They reported that the absorption rate with 0.02wt% Ag nanoparticles is enhanced by 55% compared with that of base fluid and the mass transfer performance in the binary nanofluids with the coolant is enhanced more than that without the coolant. The analysis of conjugated heat and mass transfer with a mixture ammonia-water for two modes, the falling film and the bubble absorption is carried out by Kang *et al.* (2000). They found that the local absorption rate of the bubble mode is always higher than that of the falling film mode which permits to reduce the heat exchanger size by almost 48,7%. The heat transfer coefficient had a more significant effect on the absorber size in the falling film absorption mode compared to that in the bubble mode, however the mass transfer coefficient had a more significant effect in the bubble absorption mode than in the falling film mode. In other work Fu Lin *et al.* (2011) focused on the experimental investigation of vapor absorption into LiBr solution with and without additive outside vertical tube. The enhancement of heat and mass transfer in the absorber could be obtained by adding additives such as 2-ethyl-1-hexanol to lithium bromide aqueous solution. Their results have included the effect of the inlet temperatures of LiBr solution and cooling water and the inlet concentration on mass transfer coefficient, they concluded that a strong mass transfer has occurred with 2EH. The effect of the magnetic field on the ammonia-water falling film absorption is analyzed

numerically by Xiaofeng *et al.* (2007). Their results reported that the magnetic field had a significant effect on the absorption performance of the ammonia-water falling film. Moreover, by applying a magnetic field with an intensity of 3 Tesla at the solution inlet, the concentration of ammonia-water at the outlet increases by 1.3%. A simplified model of vertical tube for the absorption of water vapor by a film of lithium bromide aqueous solution is developed by Patnaik *et al.* (1993). The model is based on the solution of differential equations to obtain the axial solution temperature and concentration distributions and the cooling water temperature distribution along a vertical absorber. They corrected the instabilities of the numerical solution at the inlet region of the tubular absorber, by introducing a dampening factor incorporating relevant thermophysical properties. It has been addressed that for the vertical tube absorber without additives, the sub-cooling has an important effect, while the addition of additives in the falling film results in an enhancement of the mass transfer coefficient, thereby reducing the effect of sub-cooling. The heat and mass transfer performance of a coiled tubular falling film absorber is studied experimentally by Tharves Mohideen and Renganarayanan (2008), by using R-134a-DMAC (1,1,1,2 Tetrafluoroethane/N-N Dimethylacetamide) solution as working fluid. For a coil absorber, the optimum overall heat transfer coefficient is 726 W/m².K for a film Reynolds number of 350. The R-134a vapor absorption rate is maximum for a coil height of 0.6 to 1. Oronel *et al.* (2013) examined an experimental study of heat and mass transfer in a vertical bubble plate absorber by using the binary (ammonia/lithium nitrate) and the ternary (ammonia/lithium nitrate-water) mixtures. The absorber used in the experiment was a corrugated plate heat exchanger with Chevron-L type corrugation (30° from the plate vertical axis). It formed by four plates, thus making three channels. The upflow of solution in the central channel was cooled by the water flowing down in the two external channels. Under the similar operating conditions, the absorption mass flux and the solution heat transfer coefficient attained with the ternary mixture are around 1.3-1.6 and 1.4 times higher respectively, than those of the binary mixture.

The presence of non-absorbable gas in an absorber is inevitable so many studies of the mechanism of the non-absorbable gas effect on the heat and mass transfer in film absorption have been published both numerically and experimentally.

Yang *et al.* (1991) investigated numerically the effects of the non-absorbable gases on the absorption heat and mass transfer rate in a smooth film. The numerical results showed that, even with a low percentage of the non-absorbable gases (0.01% of air) presented in the vapor phase, the mass transfer rate decreases significantly. A similar work is conducted by Habib and Wood (2001), with using the water-lithium bromide or water-lithium chloride as working fluid. They founded that the addition of non-absorbable gas results in a significant reduction of the absorption process. Yang (1987) analyzed

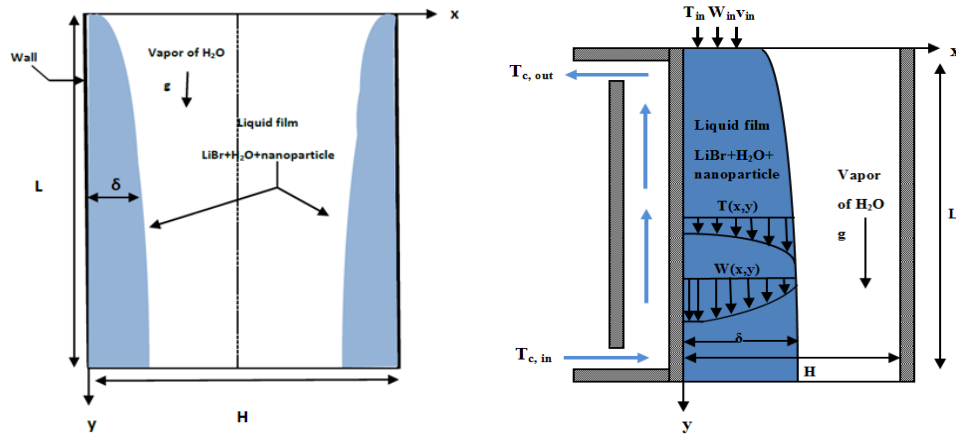


Fig. 1. Physical model.

experimentally the absorption process for a laminar wavy film of lithium chloride solution. He found that the presence of a low concentration of the non-absorbable gas leads to a decrease of the heat and mass transfer rate during absorption process. Experiments by Ameer (1992) were indicated a significant decrease in the absorption rate by increasing the non-absorbable gas concentration. For a number Reynolds of 60, he found that the reduction of the air content (non-absorbable gas) from 5 to 0.5%, has improved the absorption rate by 35%.

The present study focuses on the improvement of heat and mass transfer during absorption of vapor into liquid film along a vertical channel by adding nanoparticles to the working fluid. The binary nanofluid is LiBr-H₂O solution with nanoparticles of Ag. The conservation equations were used to determine velocity, temperature and concentration distribution within the film-thickness using the finite volume method. A parametric study to evaluate the effects of pertinent variables, such as, the volume fraction of the nanoparticles, the Reynolds number, the inlet pressure, the inlet temperature and the inlet concentration on the heat and mass transfer in falling liquid film absorption with the presence of the nanoparticles are performed.

2. PHYSICAL ABSORBER MODEL

The model of the problem studied is illustrated in Fig. 1. At the inlet of the channel, a liquid solution is introduced at a temperature T_{in} , a mass fraction W_{in} and a uniform velocity v_{in} , it flows down over vertical plate as a thin film of aqueous solution of lithium bromide, composed of absorbent (LiBr) and refrigerant (H₂O) containing nanoparticles.

The mass transfer process takes place at the interface of the aqueous solution and the water vapor coming from the evaporator. The vapor is absorbed at the interface by the film of LiBr and the heat generated due to this exothermic transformation is evacuated by the cooling water which flows in countercurrent flow to the falling liquid film inside the channel.

In formulating the mathematical model, the following assumptions have been taken into account:

- The equilibrium condition exists at the interface liquid-vapor.
- The nanoparticles are dispersed evenly in the liquid.
- The flow of liquid film is considered laminar and two dimensional.
- It was assumed that the heat transfer to the water vapor phase is negligible.
- The liquid film thickness is considered constant.
- No shear forces are exerted on the liquid film by the water vapor.
- Soret and Dufour effects are negligible.
- The radiative heat transfer is not taken into account.

3. MATHEMATICAL MODELLING

3.1 Governing Equations

Considering the above mentioned assumptions, the governing equations describing the flow, the heat and mass transfer corresponding to the continuity, momentum, energy and concentration in the liquid film can be given in the following form:

Continuity equation:

$$\frac{\partial}{\partial x}(\rho_{nf}u) + \frac{\partial}{\partial y}(\rho_{nf}v) = 0 \quad (1)$$

X-momentum equation:

$$\frac{\partial(\rho_{nf}uu)}{\partial x} + \frac{\partial(\rho_{nf}vu)}{\partial y} = \frac{\partial}{\partial x}\left(\mu_{nf}\frac{\partial u}{\partial x}\right) + \frac{\partial}{\partial y}\left(\mu_{nf}\frac{\partial u}{\partial y}\right) \quad (2)$$

Y-momentum equation:

$$\frac{\partial(\rho_{nf}uv)}{\partial x} + \frac{\partial(\rho_{nf}vv)}{\partial y} = \frac{\partial}{\partial x}\left(\mu_{nf}\frac{\partial v}{\partial x}\right) + \frac{\partial}{\partial y}\left(\mu_{nf}\frac{\partial v}{\partial y}\right) + \rho_{nf}g \quad (3)$$

Energy equation:

$$\frac{\partial\left((\rho c_p)_{nf}uT\right)}{\partial x} + \frac{\partial\left((\rho c_p)_{nf}vT\right)}{\partial y} = \frac{\partial}{\partial x}\left(k_{nf}\frac{\partial T}{\partial x}\right) + \frac{\partial}{\partial y}\left(k_{nf}\frac{\partial T}{\partial y}\right) \quad (4)$$

Concentration equation:

$$\frac{\partial(\rho_{nf}uW)}{\partial x} + \frac{\partial(\rho_{nf}vW)}{\partial y} = \frac{\partial}{\partial x}\left(\rho_{nf}D\frac{\partial W}{\partial x}\right) + \frac{\partial}{\partial y}\left(\rho_{nf}D\frac{\partial W}{\partial y}\right) \quad (5)$$

The film thickness is determined by Nusselt (1916) theory and it is described by the equation:

$$\delta = \left(\frac{3\Gamma\mu_{nf}}{\rho_{nf}^2g}\right)^{\frac{1}{3}} \quad (6)$$

3.2 Boundary Conditions

The liquid phase Eqs (1)-(5) are subjected to the following boundary conditions:

Conditions to entry: $y=0$ and $0 \leq x \leq \delta$

At the inlet of the liquid film, the temperature, concentration and velocity in the y direction of the film are uniform, while the velocity in the x direction is equal to zero.

$$T = T_{in}, \quad W = W_{in}, \quad v = v_{in} \quad \text{and} \quad u = 0 \quad (7)$$

Conditions at the wall: $0 \leq y \leq L$ and $x = 0$

At the plate wall, the no-slip and impermeable conditions are applied, so the flow velocity and the concentration gradient are equal to zero.

$$T = T_w, \quad \frac{\partial W}{\partial x} = 0, \quad v = 0 \quad \text{and} \quad u = 0 \quad (8)$$

The wall temperature changes linearly and it is calculated by the expression as follows:

$$T_w = T_{c,in} + \left(\frac{L-y}{L}\right) \times (T_{c,out} - T_{c,in})$$

Conditions at the interface: $0 \leq y \leq L$ and $x = \delta$

At the liquid-vapor interface, the interface equilibrium concentration can be obtained by a function of solution temperature and vapor pressure at the interface (McNeely 1979):

$$\text{Log}_{10}P = A + \frac{B}{T} + \frac{C}{T^2} \quad (9)$$

Where

$$A = a_0 + a_1W + a_2W^2 + a_3W^3$$

$$B = b_0 + b_1W + b_2W^2 + b_3W^3$$

$$C = c_0 + c_1W + c_2W^2 + c_3W^3$$

Equation (9) was solved iteratively using the Newton-Raphson root search method.

The interfacial absorption heat flux is determined as follows:

$$q_{surf} = k_{nf} \left. \frac{\partial T}{\partial x} \right|_{x=\delta} = \dot{m} \times h_{abs} \quad (10)$$

Where \dot{m} is the absorption mass flux of the refrigerant (water vapor) at the interface liquid-vapor and it is expressed by the following equation:

$$\dot{m} = \frac{-\rho_{nf}D}{W_{surf}} \left(\frac{\partial W}{\partial x} \right)_{x=\delta} \quad (11)$$

Continuity of shear stress:

$$\mu_{nf} \left. \frac{\partial v}{\partial x} \right|_{x=\delta} = 0 \quad (12)$$

The velocity in x-direction:

$$u = \frac{D}{W_{surf}} \left(\frac{\partial W}{\partial x} \right)_{x=\delta} \quad (13)$$

Conditions at the outlet: $y = L$ and $0 \leq x \leq \delta$

$$\frac{\partial T}{\partial y} = 0, \quad \frac{\partial W}{\partial y} = 0, \quad \frac{\partial v}{\partial y} = 0 \quad \text{and} \quad \frac{\partial u}{\partial y} = 0 \quad (14)$$

3.3 Nanofluid Properties

The thermophysical properties of Ag nanoparticles are listed in Table 1.

Table 1 Thermophysical properties of nanoparticles

Physical properties	Ag
c_p (J/kg.K)	235
ρ (kg/m ³)	10500
k (W/m.K)	429

Table 2 Comparison of local Nusselt number at the interface for various grids

				IN×JN			
y[m]	11×51	21×101	41×201	61×201	61×401	61×801	61×901
0.02	2.142	2.555	2.453	2.282	2.542	2.551	2.552
0.1	2.898	2.756	2.687	2.664	2.667	2.666	2.665
0.26	2.905	2.763	2.695	2.676	2.676	2.674	2.675
0.5	2.893	2.754	2.687	2.670	2.669	2.669	2.670
0.74	2.880	2.743	2.681	2.662	2.663	2.662	2.660
1	2.873	2.735	2.666	2.642	2.642	2.640	2.640

The density is calculated by the following (Bock 1998):

$$\rho_{nf} = (1 - \phi)\rho_f + \phi\rho_p \quad (15)$$

Where ϕ is the solid volume fraction of nanoparticles.

The nanofluid specific heat is given by Xuan and Roetzel (2000) as:

$$(\rho c_p)_{nf} = (1 - \phi)(\rho c_p)_f + \phi(\rho c_p)_p \quad (16)$$

The thermal conductivity of the nanofluid is determined by the expression proposed by Maxwell-Garnett (1904):

$$\frac{k_{nf}}{k_f} = \frac{k_p + 2k_f - 2\phi(k_f - k_p)}{k_p + 2k_f + \phi(k_f - k_p)} \quad (17)$$

The expression of dynamic viscosity of the nanofluid is approached by the Brinkman's model (1952) as follows:

$$\mu_{nf} = \frac{\mu_f}{(1 - \phi)^{2.5}} \quad (18)$$

3.4 Heat and Mass Characteristics

The total mass transfer rate absorbed and the total heat flux diffused to the liquid film are respectively defined as:

$$M_{abs} = \int_0^L \dot{m} dy \quad ; \quad Q_{surf} = \int_0^L q_{surf} dy$$

The local heat transfer coefficient from the interface to the bulk solution along the film is related to Nusselt number by the following expression:

$$Nu_{ib} = \frac{h_{ib}\delta}{k_f} = \frac{k_{nf}}{k_f} \frac{\delta}{(T_{surf} - T_{bulk})} \frac{\partial T}{\partial x} \Big|_{x=\delta}$$

The local heat transfer coefficient from the bulk solution to the wall surface along the film is related to Nusselt number by the following expression:

$$Nu_{bw} = \frac{h_{bw}\delta}{k_f} = \frac{k_{nf}}{k_f} \frac{\delta}{(T_{bulk} - T_w)} \frac{\partial T}{\partial x} \Big|_{x=0}$$

The local mass transfer coefficient from the interface to the bulk solution along the film is related to

Sherwood number by the following expression:

$$Sh = \frac{h_m\delta}{D} = \frac{\delta}{W_{surf} (W_{surf} - W_{bulk})} \frac{\partial W}{\partial x} \Big|_{x=\delta}$$

The temperature and concentration of the bulk solution are defined as follows:

$$T_{bulk} = \frac{\int_0^\delta (\rho c_p)_{nf} v T dx}{\int_0^\delta (\rho c_p)_{nf} v dx} \quad ; \quad W_{bulk} = \frac{\int_0^\delta \rho_{nf} v W dx}{\int_0^\delta \rho_{nf} v dx}$$

4. NUMERICAL PROCEDURE

4.1 Solution Method

The set of the resulting governing equations describing the heat and mass transfer and the associated boundary conditions mentioned above, are solved using the numerical finite volume method proposed by Patankar (1980). By integrating the governing differential equations, we obtained a system of algebraic equations written in the compact form as follows:

$$a_P \Phi_P = a_E \Phi_E + a_W \Phi_W + a_N \Phi_N + a_S \Phi_S + b$$

With: $\Phi = (u, v, T, W)$

The coefficients a_P, a_E, a_W, a_N, a_S are obtained by adopting the power law scheme. The resulting algebraic equations from numerical discretization are solved iteratively by the sweeping method line by line with the Thomas algorithm. The convergence of the numerical solution is declared when the maximal residual is less than 10^{-7} .

4.2 Stability of the Calculation Scheme

In order to choose a proper grid for the numerical simulation, a grid testing study was performed for seven various uniform grids: 11×51, 21×101, 41×201, 61×201, 61×401, 61×801 and 61×901. The local Nusselt number at the interface is calculated for each grid size as shown in Table 2. The results show that, the relative error is 9% for the first grid and decreases to 0.1% for the sixth grid. The obtained results allow us to conclude that the grid of 61×801 is sufficient to guarantee a grid independent solution and it is used for all results presented in this paper.

5. RESULTS AND DISCUSSION

5.1 Model Validation

In order to verify the accuracy of the present numerical procedure, a computer code was validated by comparing our present results obtained and those reported by *Yoon et al. (2005)*. Fig. 2 shows the evolution of the transverse temperature profiles of the liquid film obtained under the same conditions. A very satisfied agreement was observed between the different results. The small differences observed between the two results are less than 1%.

In this study, the numerical results for heat and mass transfer in absorption of vapor in laminar liquid film of LiBr-water with the addition of the nanoparticles are discussed. The effects of five parameters for this investigation are evaluated; these are the nanoparticles volume fraction, the Reynolds number, the inlet pressure, the inlet concentration and the inlet temperature.

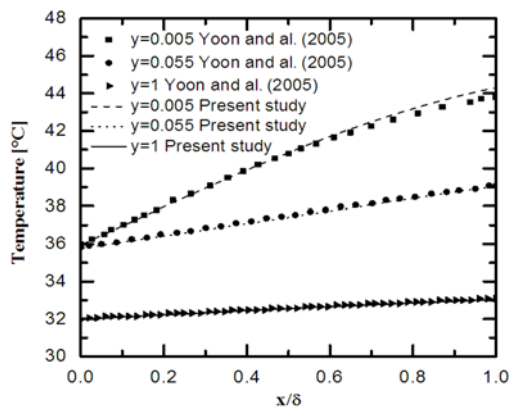


Fig. 2. Comparison of temperature profile across liquid film of present study with *Yoon et al. (2005)*.

The main parameters of operating conditions used in the calculation in the present study are presented in Table 3.

Table 3 Operating conditions

Parameters	Ranges
Inlet solution temperature T_{in}	40-60°C
Inlet solution concentration W_{in}	0.58-0.7
Reynolds number Re_{in}	10-100
Inlet pressure P_{in}	0.6-1.6KPa
Plate length L	1m
Inlet cooling water temperature $T_{c,in}$	32°C
Outlet cooling water temperature $T_{c,out}$	36°C

5.2 Influence of Nanoparticles Volume Fraction

In this section, the effect of volume fraction on the performance of the absorption is studied. Fig. 3(a) and Fig. 3(b) present respectively the distribution

of the absorption mass flux and the local Nusselt number at the interface using various volume fractions of Ag nanoparticles. Five volume fractions from 0% to 10% are considered. With the addition of nanoparticles, the absorption mass flux and the local Nusselt number from interface to liquid bulk increase as shown in Fig. 3(a) and Fig. 3(b).

Figure 3 (a) indicates that the absorption mass flux increases at the inlet and reaches a maximum. When the liquid film coming at the inlet of the channel, it starts to become cooled by cooling water, which reduces the saturation pressure and hence the absorption driving force increases and therefore the absorption mass flux increases (*Armou et al. 2016*). In addition, when the volume fraction Ag nanoparticles increases from $\phi=0$ to $\phi=0.1$, the mass flux improves by approximately 60% at the inlet of channel but, at the outlet of channel, this improvement decreases which means the end of the absorption. Same for Fig. 3(b), the local Nusselt number increases rapidly at the inlet region and by increasing the volume fraction, Nu_{ib} enhances by about 50%. So the use of nanoparticles that have a higher thermal conductivity than that of the base fluid leads to better heat transfer between the interface and the coolant (Fig. 3(b)), so, the vapor pressure driving force increases and therefore the absorption mass flux improves (Fig. 3(a)).

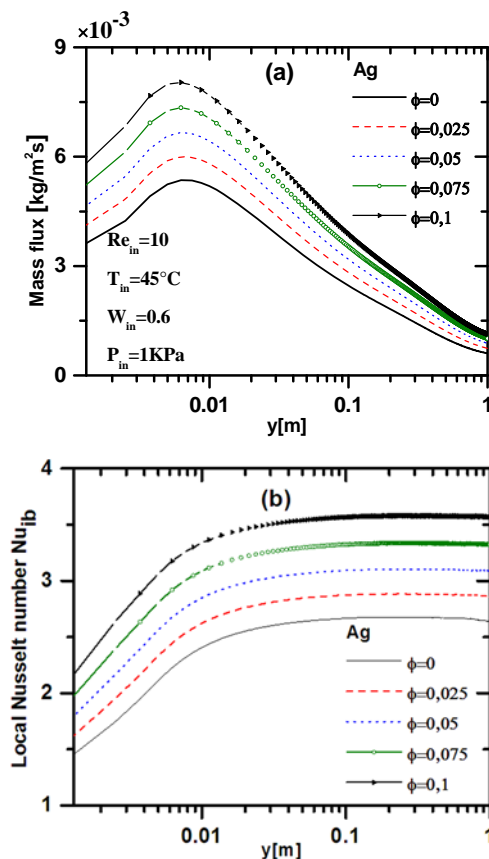


Fig. 3. Variation of (a) the absorption mass flux and (b) the local Nusselt number for various volume fractions values.

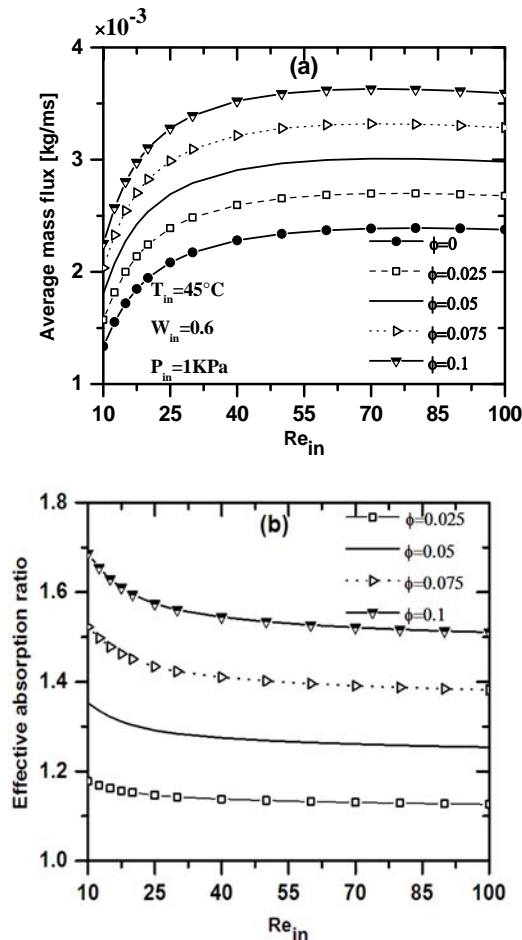


Fig. 4. (a) The average mass flux and (b) the effective absorption ratio versus Reynolds number for different volume fractions of Ag nanoparticles.

5.3 Effect of Reynolds Number

The variation of the average mass flux M_{abs} at the interface and the effective absorption ratio $R_{eff,abs}$ with the Reynolds number for LiBr-water nanofluid and LiBr-water pur is shown in Fig. 4(a) and Fig. 4(b) respectively.

Figure 4(a) indicates that M_{abs} increases with increasing Reynolds number, this increase is observed up to $Re_{in}=60$, while for Reynolds numbers higher than 60 the values of the average mass flux become almost independent of Reynolds numbers. That is explained by, the liquid film thickness increases, so the thermal resistance inhibits the cooling at the interface, which results in the elevation of the saturation pressure of the solution by accumulation of heat released at the interface, and therefore the average mass flux begins to decrease, which justifies the use of thin film absorber (Shahram *et al.* 2009).

To analyze in more detail the effect of the addition of nanoparticles on the absorption mass flux, the effective absorption ratio is expressed by Eq. (19) and it is calculated for Ag nanoparticles at different volume fractions, it remains to notice that the binary nanofluid enhances the absorption rate

when the effective absorption ratio is higher than 1.

Figure 4(b) shows that with the increase in the volume fraction, the effective absorption ratio increases and when the Reynolds number increases the effect of nanoparticles decreases the same as the improvement in absorption. With 10% of Ag nanoparticles, a significant improvement of the absorbed mass is produced with a maximum value of the effective absorption ratio of around 1.7 for the case of Reynolds number $Re_{in}=10$. Moreover, the effect of the binary nanofluid on the absorption is particularly evident at a low Reynolds number, with an improvement in the effective absorption ratio by 68% at $Re_{in}=10$ compared to 51% at $Re_{in}=100$, when the volume fraction of Ag nanoparticles increases from 0% to 10%.

The effect of the nanoparticles on the absorption mass flux is determined by the effective absorption ratio:

$$R_{eff,abs} = \frac{M_{abs,nanofluid}}{M_{abs,basefluid}} \quad (19)$$

5.4 Effect of Inlet Pressure

The average mass flux M_{abs} at the interface and the effective absorption ratio $R_{eff,abs}$ versus the inlet pressure for different concentrations of Ag nanoparticles are presented respectively in Fig. 5 (a) and Fig. 5 (b).

The pressure difference between the solution saturation pressure and the refrigerant water vapor pressure is considered a qualitative measure that describes the absorption driving force. Thus, when the inlet pressure increases, the driving potential of absorption increases so that the vapor is rapidly absorbed by LiBr solution. That is explained in Fig. 5(a), when the pressure increases, the average mass flux M_{abs} increases. Similar to the inlet pressure, the average absorption mass flux significantly increases with increasing of the volume fraction of Ag. The addition of the nanoparticles has a more apparent effect on the absorption mass flux at various values of the inlet pressure

Figure 5(b) shows the variation of the effective absorption ratio with the volume fraction Ag nanoparticles. As increasing the volume fraction of nanoparticles, the effective absorption ratio increases and becomes 67% higher with the addition of 10% volume fraction of Ag nanoparticles for all values of the inlet pressure of the solution. In this case, it can be said that the effect of the inlet pressure on the effective absorption ratio is insignificant.

The nanoparticles improve the heat and mass transfer rate by their convective characteristic such as Brownian motion. This is confirmed by the results obtained in the previous figures.

5.5 Effect of inlet Temperature

Figures 6(a) and 6(b) indicate the variation of the

mean mass flux M_{abs} at the interface and the effective absorption ratio $R_{eff,abs}$ versus the inlet temperature for each concentration of Ag nanoparticles respectively.

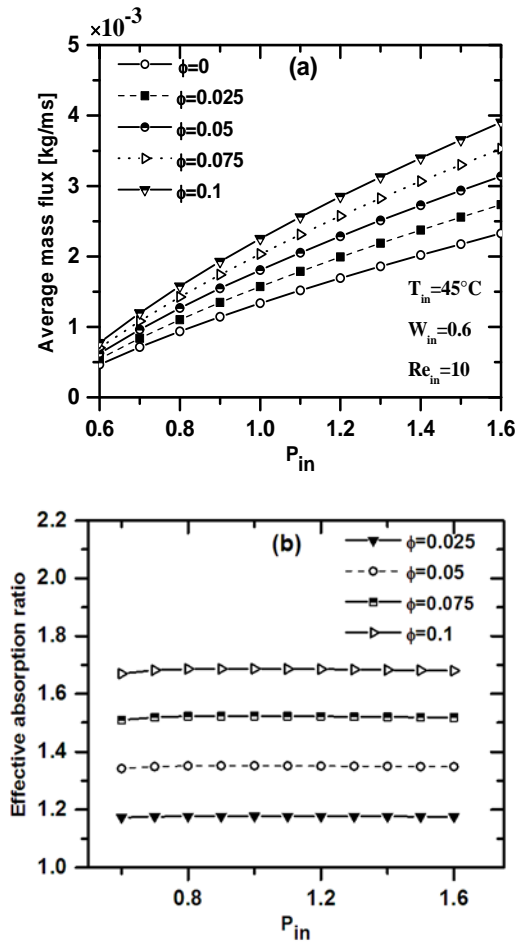


Fig. 5. (a) The average mass flux and (b) the effective absorption ratio versus inlet pressure for different volume fractions of Ag nanoparticles.

It is seen from Fig. 6(a) that the inlet temperature has a negative effect on the mass transfer performance and that the average mass flux decreases by 22% and 18% at $\phi=0$ and $\phi=0.1$ respectively when the inlet temperature of solution increases and reaches 60°C , that is due to the increase in the saturation pressure at the inlet region and therefore the vapor pressure driving force decreases and causes the average mass flux to decrease. The average mass flux demonstrates the same trend with the addition of nanoparticles. However, it can be concluded that with the increase of the inlet temperature solution, the enhancing effect induced by the addition of nanoparticles is more obvious compared to that without nanoparticles. For an inlet temperature solution that varies from 40°C to 60°C , an adding of 10% of Ag nanoparticles, increases the effective absorption ratio by 65% and 73% respectively (Fig. 6(b)).

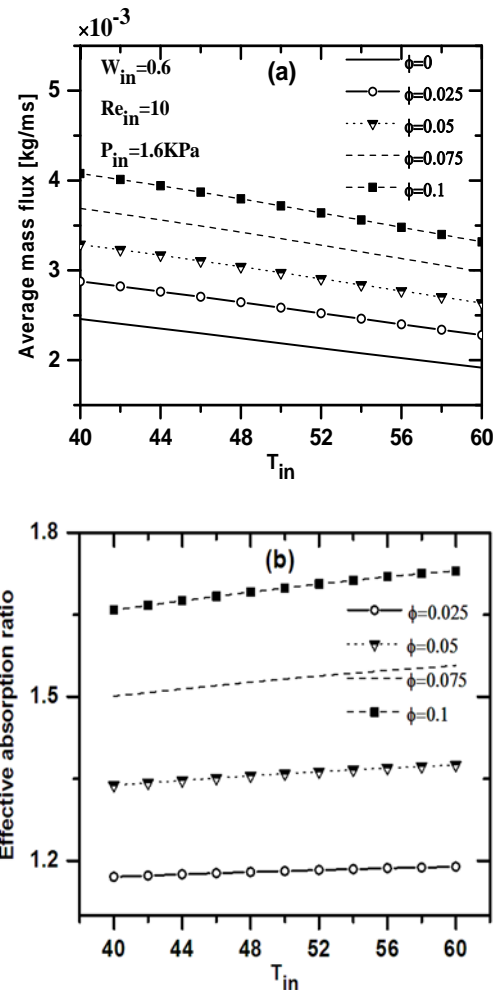


Fig. 6. (a) The average mass flux and (b) the effective absorption ratio versus inlet temperature for different volume fractions of Ag nanoparticles.

5.6 Effect of Inlet Concentration

The variation of the average mass flux M_{abs} at the interface and the effective absorption ratio $R_{eff,abs}$ versus the inlet concentration for each concentration of Ag nanoparticles are illustrated in Fig. 7(a) and Fig. 7(b), respectively.

It can be observed from the Fig. 7(a) that, the average mass flux increases with increasing the inlet concentration of LiBr and the volume fraction of nanoparticles. An increase in the inlet concentration solution reduces the solution saturation pressure and the driving force of the absorption increases, which causes an increment in average mass absorption with the presence of nanoparticles, that is due of a mass diffusion enhancement. As outlined in Fig. 7(b), it is clear that as solid volume fraction increases from 0% to 10%, the effective absorption ratio enhances by about 71% for $W_{in}=0.58$ and 46% for $W_{in}=0.7$. So when the inlet concentration is lower, the effect of the nanoparticles is more significant.

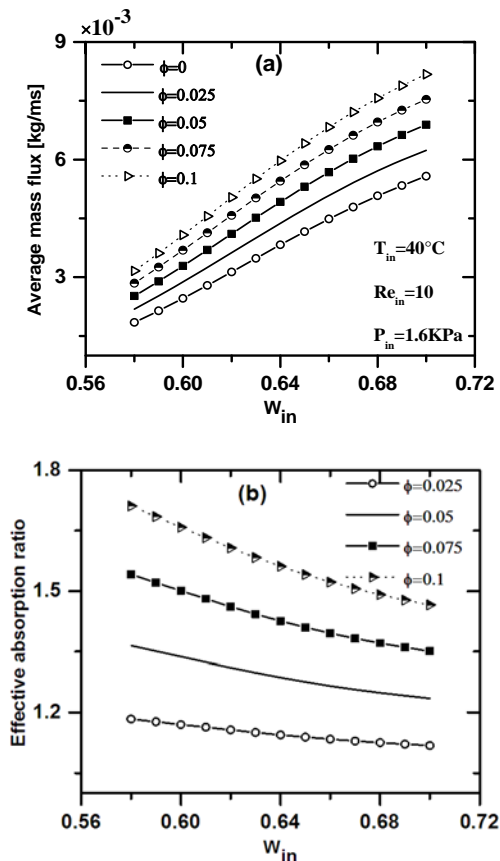


Fig. 7. (a) The average mass flux and (b) the effective absorption ratio versus inlet concentration for different volume fractions of Ag nanoparticles.

6. CONCLUSION

We studied numerically the effect of nanoparticles on heat and mass transfer during the absorption of water vapor by the aqueous solution lithium bromide along a vertical plate. The governing equations in the liquid film are discretized by the finite volume method. A validation test of numerical model was also made. The following results are drawn from this study:

- At $Re_{in}=10$, the mass and heat transfer in binary nanofluids is enhanced by 60% and 50% respectively at solid volume fraction 10% of Ag nanoparticles.
- The effect of the binary nanofluid on the absorption is particularly evident at a low Reynolds number.
- The effectiveness of the nanofluid rises with the increase in the volume fraction of nanoparticles, while it is not much affected by the inlet pressure of solution.
- It is found that the nanoparticles have a significant effect at a high inlet temperature.
- A higher value of solution concentration brings about improvement in the absorption rate of water vapor. The effect of nanoparticles is more

significant at a low value of inlet concentration.

REFERENCES

- Ameel, T. (1992). *Heat and mass transfer in laminar wavy film absorption with the presence of low concentration of non-absorbable gases*. Ph.D thesis, dissertation, Arizona State Univ., Tempe, AZ.
- Armou, S., R. Mir, Y. El hammami, S. El hamdani and K. Zine-Dine (2016). Numerical study of simultaneous heat and mass transfer in absorption of vapor in laminar liquid film. *International Journal of Enhanced Research in Science, Technology and Engineering*. 5(4), 36-47.
- Bock, C. P. and I. C. Young (1998). Hydrodynamic and heat transfer study of dispersed fluids with submicron metallic oxide particles. *Experimental Heat Transfer*. 11, 151-170.
- Brinkman, H. C. (1952). The viscosity of concentrated suspensions and solutions. *J. Chem. Phys.* 20, 571-581.
- Fu Lin, S. J. and Z. Shigang (2011). Experimental study on vertical vapor absorption into LiBr solution with and without additive. *Applied Thermal Engineering*. 31, 2850-2854.
- Habib, H. M. and B. D. Wood (2001). Simultaneous heat and mass transfer in film absorption with the presence of non-absorbable gases. *Journal of Heat Transfer*. 123, 984-989.
- Kang, Y. T., A. Akisawa and T. Y. Kashiwagi (2000). Analytical investigation of two different absorption modes: falling film and bubble types. *International Journal of Refrigeration*. 23, 430-443.
- Kim, J. K., J. Y. Jung and Y. T. Kang (2006). The effect of nano-particles on the bubble absorption performance in a binary nanofluid. *International Journal of Refrigeration*. 29, 22-29.
- Maxwell-Garnett, J. C. (1904). Colours in metal glasses and in metallic films. *Philos. Trans. R. Soc. Ser. A*. 20(3), 385-420.
- McNeely, L. A. (1979). Thermodynamic properties of aqueous solutions of lithium bromide. *ASHRAE Trans.* 85, 413-434.
- Nusselt, W. D. (1916). Oberflächenkondensation des wasserdampfes. *ZeitschrVer Deutsch.* 60, 541-546.
- Oronel, C., C. Amaris, M. Bourouis and M. Vallès (2013). Heat and mass transfer in a bubble plate absorber with $NH_3/LiNO_3$ and $NH_3/(LiNO_3-H_2O)$ mixtures. *International Journal of Thermal Sciences*. 63, 105-114.
- Pang, C., W. Wu, W. Sheng, H. Zhang and Y. T. Kang (2012). Mass transfer enhancement by binary nanofluids (NH_3/H_2O+Ag nanoparticles) for bubble absorption process. *International*

- Journal of Refrigeration*. 35, 2240-2247.
- Patankar, S. V. (1980). Numerical heat transfer and fluid flow. *Hemisphere Publishing Corporation*.
- Patnaik, V., H. Perez-Blanco and W.A. Ryan (1993). A simple analytical model for the design of vertical tube absorbers. *ASHRAE Trans.* 99(2), 69-80.
- Tharves Mohideen, S. and S. Renganarayanan (2008). Experimental studies on heat and mass transfer performance of a coiled tube absorber for R134a-DMAC based absorption cooling system. *Heat Mass Transfer*. 45, 47-54.
- Xiaofeng, N., D. Kai and D. Shunxiang (2007). Numerical analysis of falling film absorption with ammonia-water in magnetic field. *Applied Thermal Engineering*. 27, 2059-2065.
- Xuan, Y. and W. Roetzel (2000). Conceptions for heat transfer correlation of nanofluids. *International Journal of Heat and Mass Transfer*. 43(19), 3701-3707.
- Yang, R. (1987). *Heat and mass transfer in laminar wavy film absorption with the presence of non-absorbable gases*. Ph.D thesis, dissertation, Arizona State Univ., Tempe, AZ.
- Yang, R. and J. H. Chen (1991). A numerical study of the non-absorbable effects on the falling liquid film absorption. *Warme-und Stoffubertragung*. 26, 219-223.
- Yoon, J., T. Phan, C. Moon and P. Bansal (2005). Numerical study on heat and mass transfer characteristic of plate absorber. *Applied Thermal Engineering*. 25, 2219-2235.